Low-force AFM nanomechanics with higher-eigenmode contact resonance spectroscopy

Low-force AFM nanomechanics with higher-eigenmode contact resonance spectroscopy[*]

Jason P Killgore[1,2] and Donna C Hurley[1]

[1] Materials Reliability Division, National Institute of Standards and Technology, Boulder, CO, USA
[2] Department of Mechanical Engineering, University of Colorado, Boulder, CO, USA

E-mail: jason.killgore@nist.gov and

Abstract

Atomic force microscopy (AFM) methods for quantitative measurements of elastic modulus on stiff (>10 GPa) materials typically require tip–sample contact forces in the range from hundreds of nanonewtons to a few micronewtons. Such large forces can cause sample damage and preclude direct measurement of ultrathin films or nanofeatures. Here, we present a contact resonance spectroscopy AFM technique that utilizes a cantilever's higher flexural eigenmodes to enable modulus measurements with contact forces as low as 10 nN, even on stiff materials. Analysis with a simple analytical beam model of spectra for a compliant cantilever's fourth and fifth flexural eigenmodes in contact yielded good agreement with bulk measurements of modulus on glass samples in the 50–75 GPa range. In contrast, corresponding analysis of the conventionally used first and second eigenmode spectra gave poor agreement under the experimental conditions. We used finite element analysis to understand the dynamic contact response of a cantilever with a physically realistic geometry. Compared to lower eigenmodes, the results from higher modes are less affected by model parameters such as lateral stiffness that are either unknown or not considered in the analytical model. Overall, the technique enables local mechanical characterization of materials previously inaccessible to AFM-based nanomechanics methods.

S Online supplementary data available from stacks.iop.org/Nano/23/055702/mmedia

(Some figures may appear in colour only in the online journal)

1. Introduction

Originally developed for nanoscale imaging of topography, the atomic force microscope (AFM) has become a ubiquitous tool for surface and material property characterizations at the nanoscale [1, 2]. It was recognized early on that the force and lateral positioning sensitivity of the instrument could facilitate local characterization of materials' mechanical properties, especially the elastic modulus [3–5]. A particular challenge in AFM modulus measurements arises when a material's dimensions are sufficiently small that the stress field induced by the AFM tip extends through the material to the substrate or radially out from the contact to an adjacent feature [6]. Then, the measured stiffness is a convolution of the desired material beneath the contact, the deeper substrate, and the adjacent material [7, 8]. One means to address this challenge is to use lower tip–sample forces (defined here as <25 nN), resulting in a smaller stress field. Operating at low forces also has benefits for maintaining a sharp, high-resolution tip, minimizing sample damage, and characterizing near-surface property variations. Because of the deflection sensitivity limitations of the AFM, low-force static or quasistatic sample contact requires a relatively compliant cantilever. However, compliant

---

cantilevers typically lack adequate stiffness sensitivity when characterizing stiffer materials (defined here as ~10 GPa to ~1 TPa) [5]. Thus, characterization of stiffer materials has traditionally necessitated stiffer cantilevers and the correspondingly high forces that accompany them.

To understand the modulus regime that a given cantilever can probe, it is useful to consider the normalized contact stiffness $\alpha = k/k_L$, where k is the tip–sample contact stiffness and k_L is the cantilever spring constant. The finite range of α values accessible by a given cantilever is dictated by the material properties (e.g., stiffness, adhesion) and the cantilever sensitivity. When $\alpha \lesssim 1$, several AFM techniques can provide suitable stiffness sensitivity, the most widely used of which is force–distance (F–D) spectroscopy [9]. When characterizing stiff materials with F–D spectroscopy, researchers typically employ cantilevers with spring constants up to 300 N m^{-1}, resulting in typical maximum forces between 1 and 10 μN. If a compliant cantilever with $k_L = 0.2$ N m^{-1} were used to characterize the same class of materials but at much lower forces, the value of α could easily reach many hundreds or thousands. For F–D spectroscopy, such a ratio would result in a sample deformation that was undetectable relative to the cantilever deflection. Ultimately, resolving high contact stiffnesses with compliant cantilevers at low force, where $\alpha \gg 1$, demands a new set of measurement techniques.

To address the force limitations of F–D spectroscopy when characterizing stiff materials, dynamic AFM techniques have been developed. In particular, contact resonance (CR) spectroscopy techniques [10, 11] have proven well suited for modulus measurements on stiff materials. In contact resonance spectroscopy, the resonance frequency f_n^c of the nth flexural eigenmode in contact is measured. The increase in f_n^c from the resonance frequency of the corresponding mode in free space is nonlinearly proportional to the contact stiffness, with the exact relationship dependent on the cantilever geometry. With this technique, it is possible to measure the moduli of stiff materials with sufficient accuracy with the use of applied forces in the range from hundreds of nanonewtons to a few micronewtons and $\sim10 < \alpha < \sim100$ [11]. Although CR spectroscopy forces are typically much lower than those exerted in F–D measurements on the same materials, they are still sufficiently large to cause tip wear or damage [12, 13] and are too high to measure very thin films without substrate influence [8].

Contact resonance spectroscopy measurements on stiff materials typically utilize the first and/or second flexural eigenmodes of cantilevers with stiffness $k_L = 40$–50 N m^{-1} [10, 11]. In many AFM techniques, the higher eigenmodes and higher harmonics of a cantilever are useful to improve image contrast and sensitivity [14–16]. For CR spectroscopy, it was recognized early on that subsequently higher eigenmodes could provide increased frequency contrast as α is increased [17, 18]. Recently, higher CR eigenmodes have been used to characterize local mechanical property variations [19], subsurface nanoparticle dispersion [20], and nanoscale wear [13]. Such studies demonstrate the potential of higher eigenmodes in CR spectroscopy, but they do not

validate the accuracy of the results. In this paper, we use finite element analysis (FEA) to simulate contact resonance spectroscopy results for various eigenmodes and a range of values of contact stiffness. The contact resonance frequencies determined from the FEA simulation are then analyzed with a simplified analytical model (SAM) to predict values for the contact stiffness. In this way, we assess the accuracy and applicability of the SAM for low-force, higher-eigenmode contact resonance spectroscopy. With insight from the FEA results, we demonstrate higher-eigenmode measurements on samples with moduli between 50 and 75 GPa with an applied force of only 10 nN. Our results show the potential of higher-eigenmode CR spectroscopy techniques for low-force, nanomechanical characterization of nanostructured materials and devices with increased spatial resolution.

2. Feasibility of analytical analysis of higher-eigenmode CR spectra

Quantitative nanomechanical measurements with CR spectroscopy rely on analysis procedures to translate f_n^c into α. Analysis with a model based on Euler–Bernoulli beam mechanics is most commonly used [11], and this simplified analytical model (SAM) has been shown to yield accurate results with data for the lowest-order flexural eigenmode. However, the ability of the SAM to characterize the dynamics of an AFM cantilever's higher flexural eigenmodes is largely unexplored. Finite element analysis (FEA) allows for verification of the SAM while accommodating realistic cantilever geometry and properties. Compared to an experimental SAM verification scheme that must make assumptions about the beam dynamics and contact mechanics, FEA allows the tip–sample contact to be simplified to a system of elastic springs. In principle, FEA could be used to directly calculate the contact stiffness from experimental contact resonance frequencies [21–23]. However, the variability amongst different cantilevers would necessitate a unique model for every cantilever used. For experimentalists who go through numerous cantilevers over the course of a study, analytical methods are much more convenient. Thus, we seek to verify that the SAM adequately describes the dynamics of higher eigenmodes, particularly for the regime $\alpha \gg 1$ used to characterize stiff materials with compliant cantilevers and low forces.

2.1. Finite element analysis (FEA) model of a cantilever

The geometry used for the FEA model was based on a commercially available contact-mode silicon cantilever (CONT, Nanosensors, Neuchatel, Switzerland). A scanning electron microscopy (SEM) image of the cantilever is shown in figure 1(a). Although the shape is nominally rectangular, the Si etching process introduces some notable deviations from rectangularity: (1) the cross section of the cantilever is trapezoidal (not visible), and (2) the end of the cantilever comes to a triangular point. The FEA model was constructed to capture both of these deviations. A wireframe schematic of the FEA model is shown in figure 1(b) with relevant labeled
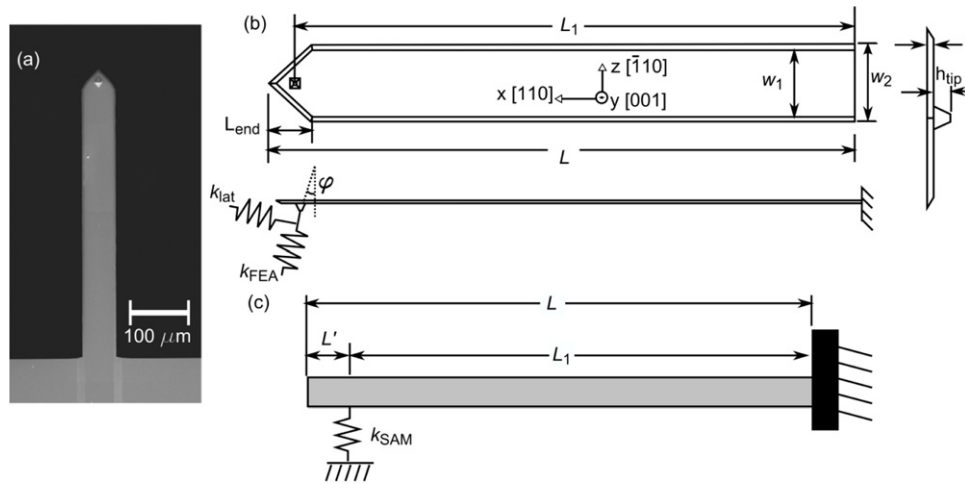
Figure 1. (a) Scanning electron micrograph of a contact-mode cantilever. (b) Finite element geometry modeled from the cantilever in (a). (c) The Euler–Bernoulli (E–B) beam model used to obtain an analytical solution for contact resonance results.

Table 1. Dimensions of the FEA cantilever model. Unless indicated otherwise, values are given in micrometers (μm).

Label	L	L_1	L_{end}	w_1	w_2	t	h_{tip}	φ
Value	439.5	419.0	32.9	45.8	52.9	1.8	6.0	11°

dimensions. The AFM tip of height h_{tip} was modeled as a truncated pyramid to eliminate the extremely small element size and large stresses that would exist if the tip were modeled as nanoscopically sharp. Values for each dimension were extracted from the SEM micrograph and are summarized in table 1.

The cantilever was modeled in Autodesk Inventor (San Rafael, CA, USA) and then imported into Ansys Workbench (Canonsburg, PA, USA). The system was automeshed with level 3 refinement, resulting in 27 258 nodes and 12 940 SOLID187 elements. The SOLID187 element is a 10-node, 3D element with quadratic displacement behavior. The silicon cantilever was modeled as anisotropically elastic, with crystallographic orientations as indicated in figure 1(b). The rotated elastic constants were Young's moduli $E_x = E_z = 169.7$ GPa, $E_y = 130.4$ GPa, Poisson's ratios $\nu_{xy} = \nu_{zy} = 0.362$, $\nu_{yz} = \nu_{yx} = 0.278$, $\nu_{xz} = \nu_{zx} = 0.061$, and shear moduli $G_{xy} = G_{yz} = 80$ GPa, $G_{zx} = 51$ GPa [23]. The density ρ was set to 2330 kg m^{-3}, and the cantilever was rigidly clamped at the back surface. As shown in figure 1(b), the tip–sample contact was modeled by two perpendicular linear springs that represent the normal and lateral stiffnesses of the contact. The normal spring was angled $\varphi = 11°$ from the horizontal (y) axis to account for the included approach angle of a typical experimental AFM cantilever holder. In a real material, the stiffness of the lateral spring k_{lat} depends on Poisson's ratio ν. Because the value of ν is not generally known, k_{lat} was set to a fraction $\lambda = k_{lat}/k_{FEA}$. The normalized lateral stiffness λ was set to either 0.65 or 1.0 to bracket the range of lateral forces that are expected for real materials with ν between 0.0 and 0.5 [24].

The free resonance frequencies f_n^0 and contact resonance frequencies f_n^c were determined from a modal analysis of the system. The free vibrations of the cantilever were determined by temporarily suppressing the contact springs. The free resonance frequencies f_n^0 of the first six eigenmodes determined in this way were $[f_1^0, f_2^0, f_3^0, f_4^0, f_5^0, f_6^0] = [12.44$ kHz, 77.79 kHz, 217.4 kHz, 425.1 kHz, 701.3 kHz, 1045 kHz]. Because the FEA model is intended to be representative of the generic class of cantilevers, rather than identical to one specific cantilever, additional dimensional refinement was not performed to match the FEA and experimental frequencies. The values of f_n^c were determined by assigning prescribed values of k_{FEA} and k_{lat} to the respective springs and performing the modal analysis. For comparison with the SAM approach described below, k_{FEA} was normalized by the spring constant k_L, and the ratio $\alpha_{FEA} = k_{FEA}/k_L$ was varied from 5×10^{-5} to 5×10^4. The spring constant k_L of the FEA cantilever was determined by applying a static load $F = 1$ nN in the y-axis direction to the truncated surface of the tip. The deflection d of the loaded surface was calculated so that $k_L = 0.16$ N m^{-1} could be determined from $k_L = \Delta F/\Delta d$.

2.2. Simplified analytical model (SAM) of a cantilever

A number of analytical models have been used to describe cantilever vibrations in CR spectroscopy, including point-mass models and beam-based models of varying complexity [11, 25, 26]. Of the beam-based models, analytical Euler–Bernoulli expressions have been most widely used. The simplest case is for a spring-coupled distributed-mass beam, parallel to the surface, with a tip of negligible height at the beam's end. More complex beam models include lateral effects, damping in the contact, tilt of the cantilever, finite tip height, and variable tip position. However, such models require a significant number of additional parameters, many of which are not easily determined. As a result, many researchers performing CR spectroscopy have adopted the model shown in figure 1(c), henceforth referred to as the simplified

analytical model (SAM), as a suitable compromise [10, 11]. This model considers a cantilever parallel to the sample surface with a spring-coupled contact located at a variable position $\gamma = L_1/L$ along the cantilever. The inclusion of variable tip position is expected to more closely describe the physical behavior of a real cantilever compared to the simpler form with $\gamma = 1$ [27].

For the system in figure 1(c), the free flexural resonance frequency f_n^0 of the nth flexural eigenmode is given by

$$f_n^0 (c_{\mathrm{B}}L)^2 = (x_n^0 L)^2 = 4\pi f_n^0 \frac{L^2}{b} \sqrt{\frac{3\rho}{E}}, \quad (1)$$

where $c_{\mathrm{B}}L$ is a cantilever parameter, and ρ, E and b are the cantilever's density, Young's modulus, and width, respectively. The scaled wavenumber $x_n^0 L$ can also be determined from the nth root of

$$1 + \cos x_n^0 L \cosh x_n^0 L = 0. \quad (2)$$

The solutions to equation (2) for the first seven eigenmodes are $[x_1^0 L, x_2^0 L, x_3^0 L, x_4^0 L, x_5^0 L, x_6^0 L, x_7^0 L] = [1.8751,$ 4.6941, 7.8548, 10.996, 14.1372, 17.2788, 20.420 36]. When the cantilever is brought in contact with the sample, the normalized contact stiffness α_{SAM} is given by

$$\alpha_{\mathrm{SAM}} = \frac{k_{\mathrm{SAM}}}{k_{\mathrm{L}}} = \frac{2}{3} (x_n L \gamma)^3 \frac{(1 + \cos x_n L \cosh x_n L)}{D}, \quad (3)$$

where k_{SAM} is the stiffness of the normal spring, $x_n L = x_n^0 L \sqrt{\frac{f_n^c}{f_n^0}}$, and D is given by

$$\begin{aligned} D = & [\sin x_n L(1 - \gamma) \cosh x_n L(1 - \gamma) \\ & - \cos x_n L\gamma \sinh x_n L\gamma][1 - \cos x_n L\gamma \cosh x_n L\gamma] \\ & - [\sin x_n L\gamma \cosh x_n L\gamma - \cos x_n L\gamma \sinh x_n L\gamma] \\ & \times [1 + \cos x_n L(1 - \gamma) \cosh x_n L(1 - \gamma)]. \end{aligned} \quad (4)$$

Thus by measuring f_n^0 and f_n^c and having a value of γ, we can find α_{SAM}. Although γ could be measured empirically with a microscope, this approach does not necessarily provide the most accurate value for analysis (see supplementary information figure S1 available at stacks.iop.org/Nano/23/055702/mmedia). Instead, it is common practice to use a 'mode-equivalence' (sometimes called mode-crossing) approach, in which we solve equations (1)–(4) for two adjacent eigenmodes (e.g., mode pairs {1, 2} or {2, 3}), then simultaneously solve for values of α_{SAM} and γ that are consistent for the mode pair [17].

The SAM analysis procedure was used to calculate values for the contact stiffness α_{SAM} from the finite element results for f_n^0 and f_n^c. Comparison of the values of α_{SAM} calculated from the analytical model with the values α_{FEA} originally imposed in the finite element model allows us to directly assess the ability of the simple SAM to describe the cantilever's behavior. In particular, it allows us to evaluate the accuracy of the SAM when using higher eigenmodes to measure contacts orders of magnitude stiffer than the cantilever spring constant k_{L}. The above SAM analysis was also used in the experimental validation experiments described in section 3 below.

### 2.3. Comparison of SAM analysis and FEA

Figures 2(a)–(e) show the relation between the contact resonance frequency f_n^c and normalized contact stiffness α determined by FEA and SAM analysis for the first five flexural eigenmodes. Each plot in figure 2 shows SAM results for a slightly different value of tip position γ that ranges from 0.982 to 0.990. These values were obtained by the mode-equivalence technique described in section 2.2 with modes pairs $\{n, n+1\}$ (for $1 \le n \le 4$) or $\{n, n-1\}$ (for $n = 5$). The values of γ were obtained at the values of α indicated by the green circle in each plot. The values were chosen in the regime where the FEA frequency results first begin to level off after their initial increase. For both analysis techniques, all modes contain a region at relatively low values of α (e.g., $\alpha \lesssim 0.1$ for $n = 1$ or $\alpha \lesssim 50$ for $n = 5$) where changes in contact stiffness have little effect on resonance frequency. At higher values of α, a regime exists where changes in contact stiffness affect f_n^c significantly. Above this region (e.g., $\alpha \gtrsim 100$ for $n = 1$ or $\alpha \gtrsim 4000$ for $n = 5$), the SAM results indicate that the frequency plateaus and becomes insensitive to changes in α. However, the more realistic FEA results demonstrate a distinct secondary regime, where increases in α produce increases in f_n^c.

The discrepancy between FEA and SAM results in the high-α regime useful for low-force CR spectroscopy is primarily attributed to the absence of a lateral spring in the SAM and its presence in the FEA model. CR spectroscopy experiments do not independently measure the lateral spring constant, making it difficult for an experimentalist to assign it a precise value. By comparing the results in figures 2(a)–(e) for $\lambda = 0.65$ and 1.0, the effect of the value of λ (and hence the value of Poisson's ratio) can be examined. Figure 2(f) summarizes these effects by plotting the difference δf between the FEA contact resonance frequencies for $\lambda = 0.65$ and 1.0. δf is defined as

$$\delta f(\alpha_{\mathrm{FEA}}, \lambda) = \frac{f_n^c(\alpha_{\mathrm{FEA}}, \lambda = 1.0) - f_n^c(\alpha_{\mathrm{FEA}}, \lambda = 0.65)}{f_n^c(\alpha_{\mathrm{FEA}}, \lambda = 1.0)}. \quad (5)$$

The smaller δf is, the less overall uncertainty there will be in the calculation of α. It can be seen from figure 2(f) that δf is as large as 2% for $n = 1$ for $500 < \alpha < 2000$ (the range of interest here), but always less than 0.5% for $n = 5$ over the same range. Although it might seem that in both cases the values of δf are small, they can correspond to large differences in the calculated values of α (e.g., for $n = 1$ and $f_1^c = 58.9$ kHz, α ($\lambda = 0.65$) is 40% larger than α ($\lambda = 1.00$)). In general, the point beyond which lateral stiffness significantly affects the f_n^c versus α relation is shifted to higher values of α for increasing eigenmode n. This behavior is attributed to the increased dynamic spring constant [15, 28] of the higher eigenmodes compared to the lower eigenmodes and the corresponding lessening of the effective ratio $k_{\mathrm{lat}}/k_{\mathrm{L}}$. Thus, with use of higher eigenmodes, sufficiently accurate values of α in the high-α regime can be obtained without precise knowledge of λ. Furthermore, comparison of the SAM and FEA results shows that despite the complete omission of the lateral spring and cantilever tilt for the SAM, the
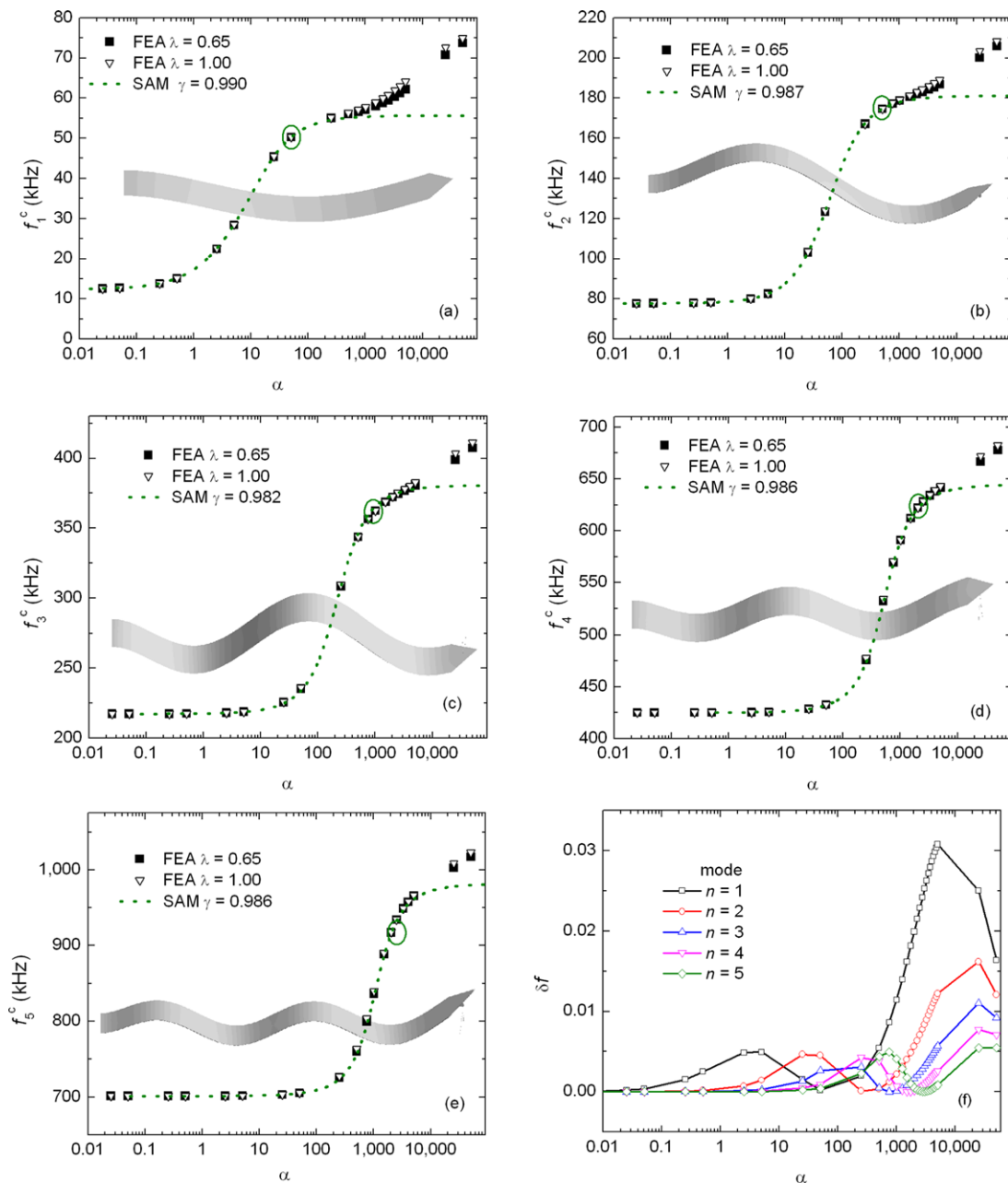
Figure 2. (a)–(e) Frequency versus normalized contact stiffness α from FEA model and SAM analysis for the first five flexural eigenmodes. FEA results (symbols) are shown for two values of the lateral-to-normal contact stiffness ratio λ. The green circles indicate the values of contact stiffness used to calculate the mode-equivalence tip position γ for the SAM. In each plot, the superimposed grayscale image shows the FEA results for the cantilever eigenmode shape for $\alpha = 1000$. (f) Normalized frequency difference δf for FEA results at the two values of λ at a given normal spring stiffness.

SAM analysis of higher eigenmodes still agrees well with the numerical FEA solution in the high-α regime of interest.

Figure 3 summarizes the ability of the SAM analysis to reproduce the FEA results. Here, the tip position γ was determined by the mode-equivalence method for each contact stiffness value. Figure 3 shows the range of contact stiffness α over which the SAM and FEA results differ by less than 10%, representing the useful stiffness range of the SAM analysis for a given mode pair $\{n, n + 1\}$. At lower contact stiffness values, the SAM results for mode pairs $\{1, 2\}$ and $\{2, 3\}$ show

better agreement with FEA than the results for the higher mode pairs $\{3, 4\}$ and $\{4, 5\}$. For the regime of high α under consideration here, the SAM and FEA results show much better agreement for the higher mode pairs. The results from mode pair $\{4, 5\}$ show less than 10% error between SAM and FEA results when $8 < \alpha_{FEA} < 3600$. In contrast, the SAM results with mode pair $\{1, 2\}$ show greater than 10% error compared to FEA results when $\alpha_{FEA} > 275$, and the error continually increases with increased stiffness. For each mode pair, the agreement between SAM and FEA drops off
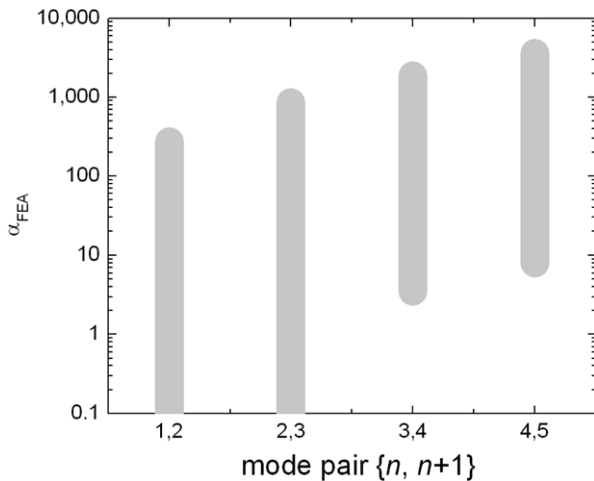
Figure 3. The bars indicate the stiffness regime over which the FEA and SAM results differ by less than 10% for the frequency versus stiffness relation.

rapidly when α_{FEA} exceeds a certain value. The breakdown in the SAM's accuracy is indicated by increasingly unphysical values of γ with increased α_{FEA}. Still higher values of α_{FEA} lead to negative values of α_{SAM}, a clear indication that the SAM is outside its useful stiffness range.

## 2.4. Eigenmode selection for SAM analysis in referencing measurements

Above we characterized the ability of the SAM to reproduce absolute values of α. Now we consider the referencing approach used in most CR spectroscopy experiments to date. If α is measured on both a reference material of known modulus and a material of unknown modulus, the unknown modulus can be calculated with only general assumptions about the tip shape [29]. Because the result depends on the ratio $\alpha(\text{unknown})/\alpha(\text{ref})$, the SAM need not accurately determine the absolute contact stiffness, as long as it correctly calculates the relative change in contact stiffness. In figures 4 and 5, we consider the case where $\alpha_{FEA}(\text{unknown})/\alpha_{FEA}(\text{ref}) = 1.25$ (indicated by the red dashed line in figure 4). Assuming a hemispherical tip, this corresponds to a ratio of indentation modulus M of $M(\text{unknown})/M(\text{ref}) \geq 1.4$, a relatively large difference.

Figure 4 shows the ability of the SAM to describe a change in contact stiffness relative to the reference contact stiffness $\alpha_{FEA}(\text{ref})$. The figure shows the value of relative contact stiffness calculated by the SAM for the same $1.25\times$ relative change in contact stiffness, but for three different values of $\alpha_{FEA}(\text{ref})$. The SAM results are calculated for mode pairs {1, 2} through {5, 6}. Similarly to figure 3, γ has been recalculated for each contact stiffness and mode pair. The lowest value, $\alpha_{FEA}(\text{ref}) = 50$, is representative of the experimental conditions that might exist when a relatively stiff cantilever ($k_L = 40$–50 N m^{-1}) is used to measure a stiff material. The highest value, $\alpha_{FEA}(\text{ref}) = 1250$, is more representative of the normalized stiffness regime under consideration here for low-force measurements of stiff

materials with compliant cantilevers. For $\alpha_{FEA}(\text{ref}) = 50$, SAM analysis calculates a ratio $\alpha_{SAM}/\alpha_{SAM}(\text{ref})$ between 1.23 and 1.26 for different eigenmode pairs, in all cases showing good agreement with the value $\alpha_{FEA}/\alpha_{FEA}(\text{ref}) = 1.25$ that was imposed in the FEA model. For $\alpha_{FEA}(\text{ref}) = 250$, the agreement between the SAM and FEA results is poorer for mode pair {1, 2} ($\alpha_{SAM}/\alpha_{SAM}(\text{ref}) = 1.17$), but is still very good for higher mode pairs. For the high-stiffness case with $\alpha_{FEA}(\text{ref}) = 1250$, the agreement between the SAM and FEA results depends considerably on the mode pair, with $\alpha_{SAM}/\alpha_{SAM}(\text{ref})$ ranging from 0.92 for $n = \{1, 2\}$ to 1.25 for $n = \{4, 5\}$, the best case.

In addition to accuracy of the analysis model, the accuracy of the experimental results also depends on a good signal-to-noise ratio. Therefore it is desirable to maximize the CR frequency shift between measurements on different materials. Figure 5 shows the frequency shift Δf between the unknown and reference materials predicted by FEA for the conditions in figure 4. Comparing figure 5 for the different reference contact stiffnesses, the maximum values of Δf are seen to occur for $n = 2$, $n = 4$, and $n = 6$ for $\alpha_{FEA}(\text{ref}) = 50$, $\alpha_{FEA}(\text{ref}) = 250$, and $\alpha_{FEA}(\text{ref}) = 1250$, respectively. For $\alpha_{FEA}(\text{ref}) = 50$, too low for characterization of stiff materials with a compliant cantilever, Δf ranges from 690 Hz for $n = 6$ to 7.5 kHz for $n = 2$. In this case ($\alpha_{FEA}(\text{ref}) = 50$), the various mode pairs yield similarly accurate values for $\alpha_{SAM}/\alpha_{SAM}(\text{ref})$. Therefore it would be most beneficial to use the mode pair {2, 3}, because these two modes exhibit the highest frequency shifts. For $\alpha_{FEA}(\text{ref}) = 1250$, within our experimental range of interest, Δf ranges from 680 Hz for $n = 1$ to 34 kHz for $n = 6$. Here the higher eigenmodes show both greater frequency shifts and improved accuracy for SAM analysis, thus limiting the usefulness of the lower modes altogether.

Figures 4 and 5 show the importance of proper mode selection for SAM analysis of CR spectroscopy experiments with $\alpha \gg 1$. In the high-stiffness regime, the SAM analysis not only matches the FEA results more closely for modes $n = 4$–6 than for lower modes, but these modes also provide significantly larger frequency shifts. By examining these results and additional ones for $\alpha_{FEA}/\alpha_{FEA}(\text{ref}) = 2$ (see supplementary information figure S2 available at stacks. iop.org/Nano/23/055702/mmedia), we can develop some guidelines for mode selection in CR experiments with SAM analysis. First, by avoiding the mode(s) with the lowest frequency contrast, one can also avoid the mode(s) for which SAM analysis yields the poorest agreement with FEA. Second, choosing the mode pair with the highest frequency shifts is expected to provide the most accurate (or nearly most accurate) results as well as the highest signal-to-noise ratio. Overall, analysis of frequency shift data for a number of eigenmodes seems to provide a simple means of choosing the modes most likely to provide SAM results consistent with FEA values.
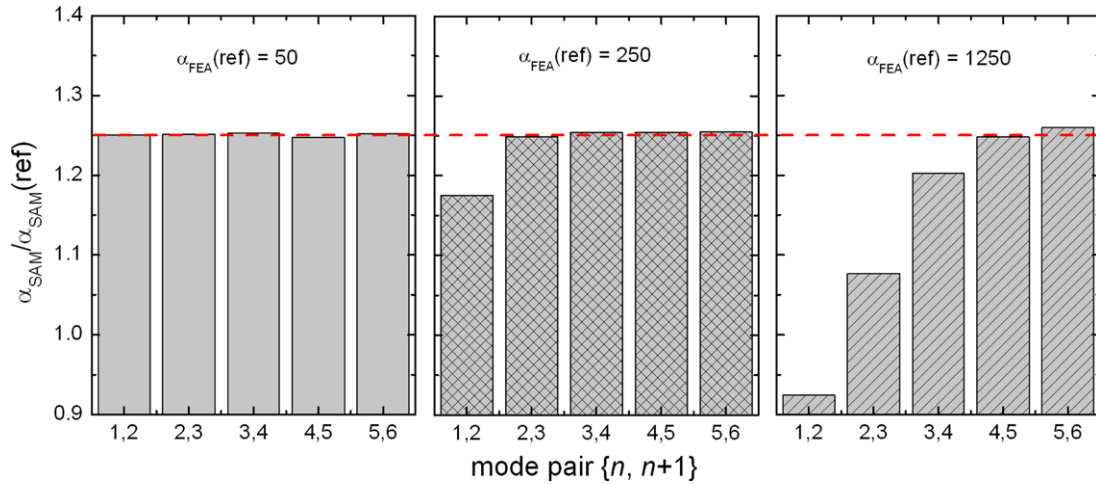
Figure 4. Results from SAM analysis and FEA for relative measurements in which the contact stiffness α of the unknown material is $1.25\times$ larger than that of the reference material. When $\alpha_{SAM}/\alpha_{SAM}(ref) = 1.25$, the SAM analysis results match those from FEA. Results are shown for $\lambda = 1.0$. The red dashed line indicates the value $\alpha_{FEA}/\alpha_{FEA}(ref) = 1.25$ imposed in the finite element model.
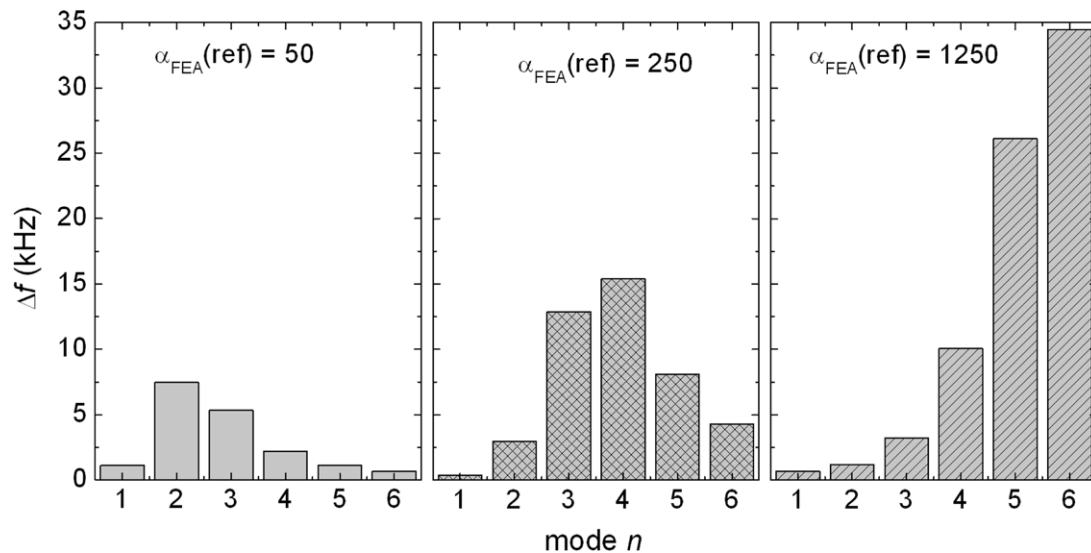
Figure 5. Frequency shift Δf from FEA for the $1.25\times$ change in contact stiffness from figure 4.

3. Application of the SAM to evaluate experimental higher-eigenmode CR spectra

3.1. Experimental setup

To demonstrate the viability of low-force, higher-eigenmode CR spectroscopy and to test our hypothesis about the relation between frequency shift and accuracy of SAM analysis, experiments were performed on fused silica glass (FSG) and 7070 lithia potash borosilicate glass (7070) (Corning Incorporated, Corning, NY) samples. Based on previous pulse-echo ultrasonic measurements, the values of the indentation moduli M were taken to be $M_{FSG} = 74.9$ GPa and $M_{7070} = 52.4$ GPa for the FSG and 7070 samples, respectively. Prior to measurement, the samples were cleaned with isopropanol, rinsed with water, and dried with compressed air.

CR spectra were acquired on an MFP-3D atomic force microscope (Asylum Research, Santa Barbara, CA) with a specialized high-frequency, heavily damped cantilever holder to excite the cantilever resonances. A CONT cantilever, similar to that which the FEA model was based on, was glued directly to the cantilever holder with fast-setting epoxy to suppress vibrational coupling at the base. From the MFP-3D's built-in thermal calibration [30], the cantilever spring constant was found to be $k_L = (0.11 \pm 0.02)$ N m^{-1}.

The free and contact resonance frequencies of the first seven flexural eigenmodes of the cantilever were determined by direct actuation of the cantilever holder. For both free and contact conditions, spectra of the cantilever vibration amplitude versus excitation frequency were obtained from 1 kHz to 1.5 MHz at as low a drive amplitude as possible to ensure linear behavior while still resolving the peaks. It was necessary to adjust the position of the laser on the

cantilever between the free and contact measurements in order to resolve the maximum number of peaks. On each of the two glasses, five contact spectra were acquired with a cantilever deflection of 94 nm, corresponding to an applied force $F_{app} = (10 \pm 2)$ nN. After acquisition of each spectrum, an adhesion force measurement was made to confirm that the adhesion force (typically 2–3 nN) was small compared to the applied force and similar for the two samples. Measurements were alternated between the two materials to reduce possible bias due to tip wear [29].

Comparison of modulus measurements from CR spectroscopy to those from bulk techniques was made with a referencing approach [29] where 7070 was the reference sample and FSG was the unknown sample. Values for the normalized contact stiffness α_{SAM} were determined for each adjacent mode pair $\{n, n \pm 1\}$. Assuming sphere–plane Hertzian contact [6], the elastic modulus was determined from measurements of α on the two samples at the same applied force by

$$\frac{\alpha(\text{unknown})}{\alpha(\text{ref})} = \frac{\alpha_{FSG}}{\alpha_{7070}} = \left(\frac{E_{FSG}^R}{E_{7070}^R}\right)^{2/3}. \qquad (6)$$

Here E^R is the reduced tip–sample modulus given by

$$\frac{1}{E^R} = \frac{1}{M_{tip}} + \frac{1}{M_{sample}}. \qquad (7)$$

The indentation modulus $M_{tip} = 165$ GPa was assumed for the [100] silicon tip. Because the contact stiffness values occur in equation (6) as a ratio, it is not necessary to determine their absolute values independently, for instance from the tip radius and the precise applied force. For the FSG and 7070 samples, we predict a contact stiffness ratio $\alpha_{FSG}/\alpha_{7070} = 1.19$.

3.2. Experimental results

Figure 6 shows representative spectra measured with the tip in free space (out of contact) and in contact with the two glasses. In free space, the lowest seven eigenmodes (with the exception of the third eigenmode) could be measured. The third mode was later measured by making small adjustments to the laser position (results not shown). In contact on either sample, the contact resonance frequencies were higher than those of the same mode for the tip in free space. For the first eigenmode, it was difficult to differentiate between the two glasses. However, for the higher modes, measurements on the FSG sample showed consistently higher frequencies than the 7070 sample. The results for the frequency shift Δf between the two samples for a given eigenmode are summarized in figure 7(a). The value of Δf was only ~32 Hz for $n = 1$, increased to almost 15 kHz for $n = 5$, and then decreased for modes 6 and 7.

Figure 7(b) shows the contact stiffness ratio $\alpha_{FSG}/\alpha_{7070}$ for the two glasses calculated with the SAM with the mode-equivalence method. The dashed line indicates the expected ratio $\alpha_{FSG}/\alpha_{7070} = 1.19$ determined from equation (6). The resonance frequencies for mode 1 were higher than the SAM
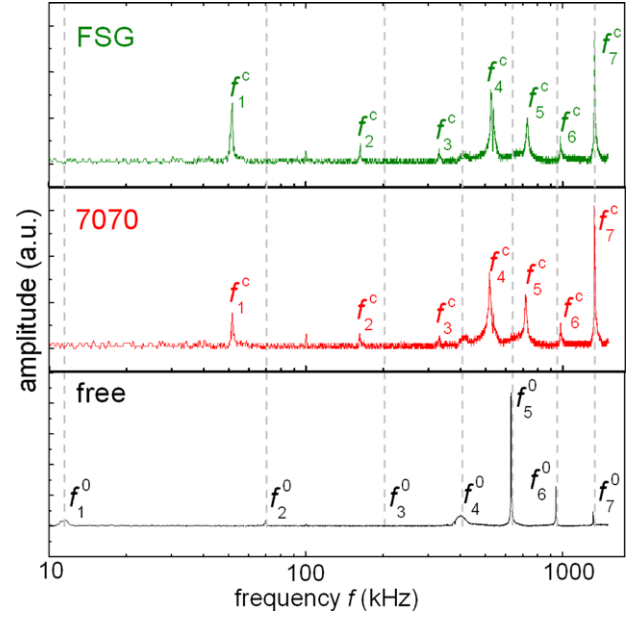

Figure 6. Experimental frequency spectra for a cantilever with $k_L = (0.11 \pm 0.02)$ N m^{-1} and an applied force of (10 ± 2) nN. The top and middle graphs show contact resonance spectra for the first seven flexural eigenmodes for fused silica glass (FSG) and 7070 glass, respectively. The bottom graph shows the free resonance spectra of the cantilever (tip out of contact).

could accommodate due to its lack of a lateral spring. As a result, physically unrealistic (negative) contact stiffness values were obtained by SAM analysis of mode 1 frequencies. Thus, the results for mode pair $\{1, 2\}$ were also negative and therefore discarded. We obtained $\alpha_{FSG}/\alpha_{7070} = 1.02 \pm 0.11$ for mode pair $\{2, 3\}$. Although the ratio correctly indicated that FSG is stiffer than 7070, the difference was much less than expected from the bulk results, and the measurement uncertainty was very large. SAM results from mode pair $\{4, 5\}$ yielded a contact stiffness ratio $\alpha_{FSG}/\alpha_{7070} = 1.17 \pm 0.03$, showing the best agreement with the predicted value of 1.19. Mode pair $\{4, 5\}$ not only provided the most accurate results in terms of agreement with bulk measurements, but it was also the mode pair with the highest frequency shifts ($\overline{\Delta f}_{4,5} = 11.6$ kHz). This is consistent with the accuracy/sensitivity guidelines proposed in section 2.4. These measurements demonstrate the power of higher-eigenmode CR spectroscopy to quantitatively probe elastic nanomechanical properties of stiff inorganic materials ($M = 50$–75 GPa) at low applied forces (~10 nN).

4. Conclusions

We have shown how the use of higher-order flexural eigenmodes ($n > 2$) in contact resonance spectroscopy enables AFM nanomechanical characterization of stiff materials with compliant cantilevers at reduced applied forces. The use of higher-order eigenmodes considerably enhances the frequency contrast on stiff materials compared to the more conventionally used lower eigenmodes ($n = 1$ or 2). Finite element analysis revealed that when analyzing
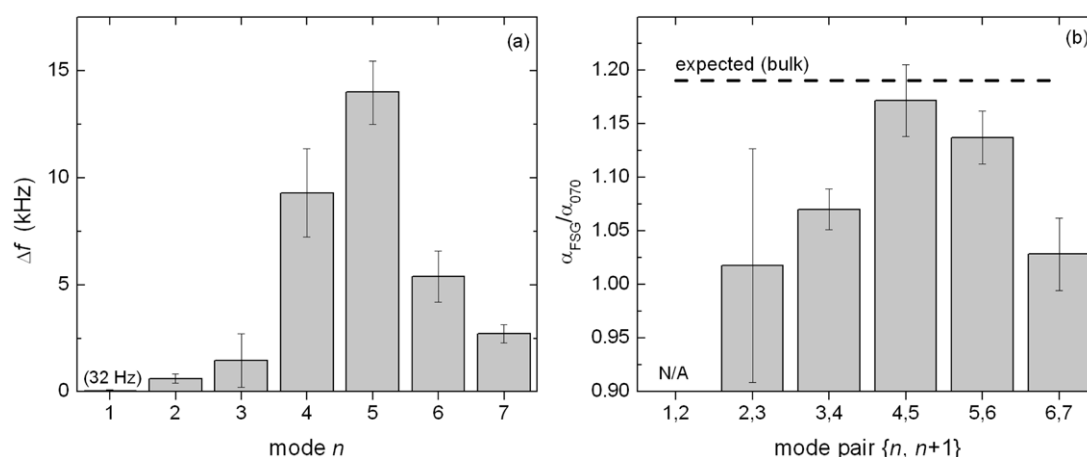
Figure 7. (a) Experimental contact resonance frequency shift Δf between fused silica glass and 7070 glass versus flexural eigenmode number n. (b) Contact stiffness ratio $\alpha_{FSG}/\alpha_{7070}$ versus mode pair $\{n, n+1\}$ calculated from the experimental frequencies with SAM analysis. The dashed line indicates the value $\alpha_{FSG}/\alpha_{7070} = 1.19$ expected from bulk measurements. The result for mode pair $\{1, 2\}$ gave negative contact stiffness and was omitted.

higher-eigenmode results for large contact stiffnesses, the effect of unknown experimental parameters, such as lateral contact stiffness, on the calculated contact stiffness was considerably reduced. By comparison with results from finite element analysis (FEA), we demonstrated that a simplified analytical model (SAM) can yield sufficiently accurate values of contact stiffness that are orders of magnitude larger than the cantilever's spring constant. However, the SAM analysis reproduced the FEA results within acceptable limits (difference $< 10\%$) only over a specific contact stiffness regime that depended on the specific eigenmode. The FEA results suggest that the optimal eigenmodes for SAM analysis conveniently correspond to the eigenmodes that produce the largest frequency shifts between the materials of interest. More advanced models that consider lateral stiffness and tilt might extend the stiffness regime that can be analyzed to yield sufficiently accurate results for a particular mode pair. However, even using these advanced analytical models, we could not determine parameter values that provided good agreement with the FEA results for all modes and all values of α. Insight gained from the FEA results allowed us to demonstrate accurate modulus measurements on stiff samples with an applied force of only 10 nN through use of the fourth and fifth eigenmodes of a cantilever 400 times more compliant than those typically used in CR spectroscopy. The ability to characterize nanomechanical properties of stiff materials at such low forces will be of significant benefit in the characterization of ultrathin films and nanostructures, where measurements with higher force techniques are heavily affected by substrate and boundary effects.

Acknowledgments

References

[1] Durig U 1999 *Appl. Phys. Lett.* **75** 433–5
[2] Hoelscher H, Allers W, Schwarz U D, Schwarz A and Wiesendanger R 1999 *Phys. Rev. Lett.* **83** 4780–3
[3] Pethica J B and Oliver W C 1987 *Phys. Scr.* **T19A** 61–6
[4] Burnham N and Colton R 1989 *J. Vac. Sci. Technol.* A **7** 2906–13
[5] Maivald P *et al* 1991 *Nanotechnology* **2** 103–6
[6] Johnson K L 1985 *Contact Mechanics* (Cambridge: Cambridge University Press)
[7] Clifford C A and Seah M P 2006 *Nanotechnology* **17** 5283–92
[8] Kopycinska-Müller M, Striegler A, Kahler B and Wolter K-J 2011 *Adv. Eng. Mater.* **13** 312–8
[9] Butt H J, Cappella B and Kappl M 2005 *Surf. Sci. Rep.* **59** 1–152
[10] Rabe U 2006 *Applied Scanning Probe Methods II* ed B Bushan and H Fuchs (Berlin: Springer) pp 37–90
[11] Hurley D C 2009 *Applied Scanning Probe Methods XI* ed B Bushan and H Fuchs (Berlin: Springer) pp 97–138
[12] Kopycinska-Müller M, Geiss R H and Hurley D C 2006 *Ultramicroscopy* **106** 466–74
[13] Killgore J P, Geiss R H and Hurley D C 2011 *Small* **7** 1018–22
[14] Stark R W and Heckl W M 2003 *Rev. Sci. Instrum.* **74** 5111–4
[15] Melcher J, Hu S and Raman A 2007 *Appl. Phys. Lett.* **91** 053101
[16] Martinez-Martin D, Herruzo E T, Dietz C, Gomez-Herrero J and Garcia R 2011 *Phys. Rev. Lett.* **106** 198101
[17] Rabe U, Amelio S, Kester E, Scherer V, Hirsekorn S and Arnold W 2000 *Ultrasonics* **38** 430–7
[18] Turner J A and Wiehn J S 2001 *Nanotechnology* **12** 322–30
[19] Nair S S, Wang S and Hurley D C 2010 *Composites* A **41** 624–31
[20] Killgore J P, Kelly J Y, Stafford C M, Fasolka M J and Hurley D C 2011 *Nanotechnology* **22** 7
[21] Arinero R and Lévêque G 2003 *Rev. Sci. Instrum.* **74** 104

[22] Beltran F J E, Munoz-Saldana J, Torres-Torres D, Torres-Martinez R and Schneider G A 2006 *J. Mater. Res.* **21** 3072–9

[23] Espinoza-Beltran F J, Geng K, Muñoz Saldaña J, Rabe U, Hirsekorn S and Arnold W 2009 *New J. Phys.* **11** 083034

[24] Wright O B and Nishiguchi N 1997 *Appl. Phys. Lett.* **71** 626–8

[25] Rabe U, Turner J and Arnold W 1998 *Appl. Phys.* A **66** S277–82

[26] Stan G and Cook R F 2008 *Nanotechnology* **19** 10

[27] Rabe U, Janser K and Arnold W 1996 *Rev. Sci. Instrum.* **67** 3281

[28] Lozano J R, Kiracofe D, Melcher J, Garcia R and Raman A 2010 *Nanotechnology* **21** 465502

[29] Rabe U, Amelio S, Kopycinska M, Hirsekorn S, Kempf M, Goken M and Arnold W 2002 *Surf. Interface Anal.* **33** 65–70

[30] Hutter J L and Bechhoefer J 1993 *Rev. Sci. Instrum.* **64** 1868–73